ARTICLE IN PRESS

Nature Communications

https://doi.org/10.1038/s41467-026-69837-8

Article in Press

From the same supramolecular framework to distinct types of porous liquids via in-situ transformation

Received: 14 May 2025

Accepted: 11 February 2026

[redacted]

Cite this article as: Liu, Y., Jin, H.-Y., Li, M.-M. *et al.* From the same supramolecular framework to distinct types of porous liquids via in-situ transformation. *Nat Commun* (2026). https://doi.org/10.1038/s41467-026-69837-8

Yang Liu, Han-Yan Jin, Meng-Meng Li, Tao Yang, Mingrui Zuo, Chenrui Li, Lifeng Ding & Lin-Bing Sun

We are providing an unedited version of this manuscript to give early access to its findings. Before final publication, the manuscript will undergo further editing. Please note there may be errors present which affect the content, and all legal disclaimers apply.

If this paper is publishing under a Transparent Peer Review model then Peer Review reports will publish with the final article.

ARTICLE IN PRESS

© The Author(s) 2026. **Open Access** This article is licensed under a Creative Commons Attribution-NonCommercial-NoDerivatives 4.0 International License, which permits any non-commercial use, sharing, distribution and reproduction in any medium or format, as long as you give appropriate credit to the original author(s) and the source, provide a link to the Creative Commons licence, and indicate if you modified the licensed material. You do not have permission under this licence to share adapted material derived from this article or parts of it. The images or other third party material in this article are included in the article's Creative Commons licence, unless indicated otherwise in a credit line to the material. If material is not included in the article's Creative Commons licence and your intended use is not permitted by statutory regulation or exceeds the permitted use, you will need to obtain permission directly from the copyright holder. To view a copy of this licence, visit http://creativecommons.org/licenses/by-nc-nd/4.0/.

From the same supramolecular framework to distinct types of porous liquids via in-situ transformation

Yang Liu[1,2], Han-Yan Jin[1,2], Meng-Meng Li[1,2], Tao Yang[1,2], Mingrui Zuo[3], Chenrui Li[3], Lifeng Ding[3], and Lin-Bing Sun[1,2★]

[1] State Key Laboratory of Materials-Oriented Chemical Engineering, Nanjing Tech University, Nanjing 211816, China. [2] College of Chemical Engineering, Nanjing Tech University, Nanjing 211816, China. [3] Department of Chemistry and Materials Science, Advanced Materials Research Center, School of Science, Xi'an Jiaotong-Liverpool University, Suzhou 215123, China. ★Email: lbsun@njtech.edu.cn.

Abstract

Porous liquids (PLs), integrating porous hosts into flowing liquids through intermolecular interactions, attract significant attention, while their controlled synthesis remains challenging. Here we report a controllable in-situ transformation strategy to fabricate distinct types of PLs from the same supramolecular framework (SMF). Two isomorphic polyethylene-glycol-based ionic liquids, IL-Br and IL-NTf$_2$, differing only in anions, exhibit contrasting electrostatic interactions with the SMF. Strong attraction between IL-Br and the SMF disrupts the ionic bonds within the framework, yielding a type II PL, PL2(SMF–Br), while electrostatic repulsion in IL-NTf$_2$ preserves the framework, producing a type III PL, PL3(SMF–NTf$_2$). These tailored host–solvent interactions endow PL2(SMF–Br) with over twice the CO$_2$ uptake and photoresponsivity of its counterpart, as well as record-high CO$_2$ capacity among reported type II PLs. In this work, we establish a general strategy for tunable PL construction through electrostatically guided host–solvent design.

Introduction

Porous liquids (PLs), which ingeniously combine fluidity and porosity, have inspired researchers to develop diverse design strategies for their fabrication.[1-4] These materials consist of two primary components: porous hosts that provide porosity and sterically hindered solvents that ensure fluidity.[5-9] According to the interactions between these components, PLs are classified into three types.[10,11] Type I PLs are single-component fluids where the solvents are chemically bonded to the porous hosts.[12-16] Type II PLs are homogeneous solutions formed by dissolving porous hosts in sterically hindered solvents.[17,18] Type III PLs consist of porous materials uniformly dispersed in such solvents.[19-26] Due to the complexity of forming stable chemical bonds in type I PLs, more attention has been paid to type II and type III PLs.

The design and synthesis of type II and type III PLs require careful selection of different porous hosts based on their interaction with sterically hindered solvents.[27-29] For type II PLs, the porous hosts must dissolve in the solvents, which favors smaller, discrete structures such as porous organic cages (POCs)[30-32] and metal-organic cages (MOCs).[33-36] In contrast, type III PLs rely on the uniform dispersion of porous materials within the solvents, typically using three-dimensional frameworks such as metal-organic frameworks (MOFs),[37-41] covalent organic frameworks (COFs),[42] zeolites,[43,44] and porous carbon materials.[45,46] Hence, the synthesis of type II and type III PL primarily relies on porous hosts with significant structural differences. This approach complicates the elucidation of the underlying synthetic mechanisms and hinders direct comparisons of the properties of PLs with different types. Albeit interesting and highly expected, the controlled fabrication of different types of PLs using the same porous host has never been reported.

In this work, we present an in-situ transformation strategy to achieve controllable synthesis of different types of PLs from the same porous host, supramolecular framework (SMF) (Fig. 1). SMFs constructed from the hierarchical self-assembly of MOCs via ionic bonds represent an emerging frontier in materials research. Given the relatively low energy of ionic bonds, it becomes possible to regulate the properties of sterically hindered solvents, thereby preserving or disrupting these ionic bonds to achieve controllable preparation of type III or type II PLs. Based on the characteristic of SMFs, two isomorphic polyethylene glycol-based ionic liquids with Br^- and trifluoromethanesulfonyl (NTf_2^-) as counteranions are designed and synthesized as sterically hindered solvents, denoted as IL-Br and IL-NTf_2, respectively. In the solvent IL-NTf_2, the primary structure of SMF is preserved and the porous host can be dispersed, enabling the successful synthesis of type III PL denoted as PL3(SMF-NTf_2). Interestingly, ionic bonds within the SMF are disrupted in IL-Br, leading to the in situ transformation of SMFs into discrete MOCs that dissolve completely, yielding type II PL denoted as PL2(SMF-Br) with a high solubility (150 g L^{-1}) among type II PLs. Further studies reveal that the SMF surface carries positive charge, while IL-Br is negatively charged, facilitating dissolution; meanwhile, IL-NTf_2 is positively charged, allowing the SMF to remain uniformly dispersed. It is noteworthy that PL2(SMF-Br) exhibits CO_2 adsorption capacity of 21.6 cm^3 g^{-1} at 0 °C and 1 bar, which is more than twice of its type III counterpart PL3(SMF-NTf_2) (10.1 cm^3 g^{-1}) and is the highest among all reported type II PLs. Due to the presence of photoresponsive motifs, PL2(SMF-Br) shows 43.0% of CO_2 uptake change under light irradiation, which is obviously larger than that of PL3(SMF-NTf_2) (21.7%). We also demonstrate that the present in-situ transformation strategy can be extended to synthesize other PLs with different types from the same porous hosts.

Results

Controllable synthesis of different types of PLs from the same porous host. The SMF was synthesized through self-assembly of zirconium dichlorocene (Cp_2ZrCl_2) with carboxylic acid ligands, 2-(2-phenyldiazenyl)-1,4-benzenedicarboxylic acid (H_2BDC-Azo), via MOC as intermediate (Fig. 1a and Supplementary Fig. 1). A comprehensive array of characterization techniques, including electrospray ionization mass spectrometry (ESI-MS), powder X-ray diffraction (PXRD), and scanning electron microscopy (SEM), were employed to validate the successful synthesis of SMF (Supplementary Figs. 2-4). The resulting SMF features a three-dimensional structure composed of orthotetrahedral MOCs interconnected by Cl^-. Each MOC within SMF is distinguished by four equilateral triangular windows, with side lengths of 11.2 Å, and an internal cavity measuring 8.5 Å in diameter. The interaction inside SMF inspired us to design sterically hindered solvents, aiming to preserve or disrupt the ionic bonds to achieve controlled preparation of type III or type II PLs.

A bimidazolium ionic liquid, IL-Br, based on the low-viscosity polymer polyethylene glycol is designed and synthesized with a size of 3.75 × 1.86 × 1.12 nm^3 (Supplementary Fig. 5). Ion exchange is then employed to replace the counteranion Br^- with NTf_2^-, yielding IL-NTf_2 with a size of 3.75 × 1.86 × 1.41 nm^3 (Fig. 1b and Supplementary Figs. 6-7). These ionic liquids exceed the window size of the cage, making them sterically hindered solvents for the synthesis of PLs. Although ionic liquids are overall electrically neutral, their intrinsic ionicity leads to charge localization, thereby promoting electrostatic interactions between the ionic liquid and the porous host.[47,48] Interestingly, SMF dissolved effectively in IL-Br, forming a red transparent solution, which is categorized as a type II PL. In contrast, mixing SMF with IL-NTf_2 results in an opaque yellow suspension, characteristic of a type III PL (Fig. 1b and Supplementary Fig. 8). The structural integrity of SMF within PLs is assessed using PXRD. A distinct diffraction peak characteristic of SMF is observed in the PL3(SMF-NTf_2), confirming that SMF remains structurally intact in this PL. Macroscopically, PL2(SMF-Br) appears optically transparent, indicating that the crystalline SMF framework has disassembled. This is further confirmed by the amorphous pattern observed in the PXRD (Fig. 2a). Meanwhile, characteristic peaks corresponding to the MOC species are still detected in the ESI-MS spectra, confirming that the discrete MOC units remain intact, thereby suggesting the successful transformation of SMF into soluble MOCs (Supplementary Figs. 9-11).

The mechanisms underlying the interactions between SMF and sterically hindered solvents are investigated. Zeta potential is a key indicator of surface charge, providing insight into the interactions between different components.[49,50] Analysis shows that IL-Br has a zeta potential of -5.6 mV, while IL-NTf_2 exhibits a potential of +1.6 mV, indicating opposite surface charges. Meanwhile, SMF exhibits a potential of +8.7 mV (Fig. 2b). The electrostatic attraction between negatively charged IL-Br and positively charged SMF promotes the in-situ transformation of SMF to MOCs and subsequent dissolution, leading to the formation of type II PL. In addition, the isolated MOC exhibits a much higher zeta potential of +44.3 mV, attributed to its more exposed active sites. This stronger electrostatic interaction with IL-Br further drives the transformation process (Supplementary Fig. 12). Notably, the solubility reaches 150 g L^{-1} in IL-Br, which is higher than most reported MOC-based type II PLs (2–62 g L^{-1}; Fig. 2c and Supplementary Table 1). In contrast, the similar positive surface charges of SMF and IL-NTf_2 create repulsive interactions, leading to the formation of a stable dispersed type III PL. ^{1}H NMR spectroscopy provides further insights into the interactions between components. The characteristic peaks of the sterically hindered solvents in PL2(SMF-Br) and PL3(SMF-NTf_2) remain prominent due to their high proportion. After introducing SMF, the peaks of the ionic liquids shift to varying extents, with the most significant shifts observed in the imidazole region (Supplementary Figs. 13-14). This suggests that the porous host interacts most strongly with the imidazole moiety of the ionic liquids. Notably, the imidazole peak in PL2(SMF-Br) shifts by 0.15 ppm, compared to a 0.08 ppm shift in PL3(SMF-NTf_2), indicating a stronger interaction between IL-Br and the porous host than with IL-NTf_2 (Fig. 2d). Interestingly, the shift in PL2(SMF-Br) is upfield, suggesting that SMF donates electrons to the imidazole moiety of IL-Br, increasing its electron cloud density. In contrast, the downfield shift in PL3(SMF-NTf_2) indicates that SMF exerts an electron-withdrawing effect on the imidazole group of IL-NTf_2, reducing its electron cloud density.

Simulations results further clarify the difference in interaction strength by quantifying the interaction energies (ΔE). The calculated ΔE between MOC and Cl^- is -52.9 kcal mol^{-1} (Fig. 2e and Supplementary Table 2), significantly weaker than the -90.7 kcal mol^{-1} observed between IL-Br and MOC (Fig. 2f). This stronger affinity facilitates the disruption of intermolecular forces within SMF, promoting the formation of a type II PL. In contrast, the interaction energy between IL-NTf_2 and MOC is only -40.1 kcal mol^{-1}, substantially weaker than the ΔE between MOC and Cl^- (Fig. 2g). This weaker interaction energy suggests that IL-NTf_2 lacks the ability to effectively disrupt the SMF structure, leading to the formation of a type III PL.

Characterization of the obtained type II and III PLs. The presence of permanent cavities is a critical factor in the successful synthesis of PLs. To verify the existence of such intrinsic porosity, positron annihilation lifetime spectroscopy (PALS) measurements were performed to determine the τ3 lifetime. The results reveal that, compared with pure IL-Br, τ3 increases from 2.185 ns in IL-Br to 2.489 ns in PL2(SMF-Br). Similarly, τ3 rises from 2.995 ns in IL-NTf$_2$ to 3.105 ns in PL3(SMF-NTf$_2$). These increases in τ3 provide direct evidence that the incorporation of SMF introduces permanent cavities into the liquid phase (Supplementary Fig. 15). Meanwhile, molecular dynamics (MD) simulations were performed to examine the spatial relationship between IL and MOC. Due to the conformational flexibility of azobenzene units, MOCs exist in both trans-MOC and cis-MOC forms under different conditions.[51,52] Simulations reveal that IL-Br remains restricted to the exterior of trans-MOC without penetrating its cavity (Supplementary Movie 1). This is further supported by radial distribution function (RDF) analysis between the center of trans-MOC and IL-Br (two imidazolium rings and the center of chain), which shows that IL-Br is confined to a range of r = 9.9–14.9 Å, well beyond the cage radius of 4.3 Å (Fig. 3a). This restricted motion confirms that IL-Br does not enter the inner cavities, verifying the successful synthesis of type II PL. To assess whether this structural transformation impacts the porosity, similar simulations were performed for cis-MOC. The results indicate that IL-Br remains excluded from the cavity (Supplementary Fig. 16 and Supplementary Movie 2), further confirming the permanent porous structure. To simplify the simulation of SMF and IL-NTf$_2$, the same computational approach was applied as for MOC and IL-NTf$_2$, given that the porosity of SMF primarily originates from the MOC. The objective was to determine whether IL-NTf$_2$ could enter the cavities of MOC. The results confirm that IL-NTf$_2$ also remains outside the trans-MOC cavity (Fig. 3b). RDF analysis between the center of trans-MOC and IL-NTf$_2$ (two imidazolium rings and the center of chain) shows that IL-NTf$_2$ is constrained to a range of r = 10.3–14.3 Å, reinforcing its exclusion from the cavity and confirming the successful synthesis of type III PL (Supplementary Movie 3). Even after azobenzene isomerization, the cis-MOC cavity remains intact, ensuring that the porous structure is maintained (Supplementary Fig. 17 and Movie 4).

The physicochemical properties of PLs were thoroughly characterized. Thermal stability analysis indicates that PLs exhibit similar stability to their sterically hindered solvent counterparts, indicating the introduction of porous host does not compromise the thermal stability (Fig. 3c). Viscosity, a measure of internal molecular friction, provides insight into intermolecular interactions.[53] PL2(SMF-Br) exhibits a viscosity of 93.8 Pa·s at 0 °C, which is 2.4 times higher than that of pure IL-Br (39.6 Pa·s). In contrast, PL3(SMF-NTf$_2$) has a viscosity of 4.7 Pa·s, comparable to that of IL-NTf$_2$ (4.5 Pa·s). This lower viscosity is attributed to intermolecular repulsive forces, which contribute to a lubricating effect within the system[50] (Fig. 3d). The significantly higher viscosity of PL2(SMF-Br) suggests stronger attractive forces and greater intramolecular friction compared to PL3(SMF-NTf$_2$). Despite this, both PLs retain good flowability at 0 °C due to the inherently low viscosity of polyethylene glycol-based ionic liquids.[54] Oscillatory rheology experiments confirm their liquid-like behavior, with the loss modulus (G″) exceeding the storage modulus (G′). Notably, PL2(SMF-Br) exhibits a higher G″ than PL3(SMF-NTf$_2$), indicating a more stable system consistent with its higher viscosity (Fig. 3e).

Given that SMF is constructed from azobenzene ligands, the synthesized PLs may inherit photoresponsive properties. Upon exposure of PL2(SMF-Br) to UV light (365 nm), the absorbance at 322 nm rapidly decreases, while the absorbance at 412 nm increases (Supplementary Fig. 18). This behavior results from azobenzene isomerization from trans to cis, altering electronic transitions from π-π* to n-π*. The isomerization occurs rapidly, with significant absorbance changes within 5 min, corresponding to a photoisomerization proportion of 29.8% (Fig. 3f). Similarly, PL3(SMF-NTf$_2$) exhibits a decrease in absorbance at 322 nm and an increase at 412 nm under identical UV light, indicating a similar isomerization process. However, its photoisomerization proportion is significantly lower (8.9%) in comparison with that of PL2(SMF-Br) (Supplementary Fig. 19). Normalized absorbance values (Fig. 3f) suggest that differences in states influence photoresponsiveness. In PL2(SMF-Br), where individual cages are dispersed, isomerization is more efficient due to minimal steric resistance. In contrast, in PL3(SMF-NTf$_2$), where SMF forms an extended framework, backbone rigidity and reduced UV transmittance hinder isomerization, resulting in a lower proportion. Switching to visible light (Vis, 420 nm) reverses the photoisomerization of PL2(SMF-Br), with absorbance at 322 nm returning to its initial state within 1 min (Supplementary Fig. 20), demonstrating rapid and reversible switching (Fig. 3f). Similarly, PL3(SMF-NTf_2) also exhibits reversible isomerization under Vis light (Supplementary Fig. 21). Continuous UV-Vis light cycles confirm that both PLs maintain stable absorbance changes, demonstrating fully reversible trans/cis isomerization (Supplementary Figs. 22–23). This reversibility highlights the potential of these materials for applications requiring responsive molecular switching.

Gas adsorption behavior of the obtained type II and III PLs. Rising atmospheric CO_2 levels drive climate change, disrupting ecosystems and human activities.[55-57] Much attention has been paid to adsorptive carbon capture, and the CO_2 adsorption behavior of the obtained PLs were evaluated. As the concentration of porous host increased, the CO_2 adsorption capacity first increased and then decreased on type II PLs. The optimum PL2(SMF-Br) sample with the concentration of 7% presents the CO_2 uptake of 21.6 cm^3 g^{-1} at 1 bar and 0 °C. However, when the concentration above 7%, adsorption capacity declined (Supplementary Figs. 24–28). This decline is attributed to molecular-level aggregation of MOCs at higher concentrations,[58] which blocks adsorption sites.[35] Notably, PL2(SMF-Br) exhibits the highest CO_2 adsorption capacity among all reported type II PLs (0.16–13.5 cm^3 g^{-1}) under comparable conditions (Supplementary Table 3 and Fig. 4c), also significantly outperforming pure IL-Br (2.6 cm^3 g^{-1}) (Supplementary Fig. 29). Similarly, PL3(SMF-NTf_2) achieves a CO_2 adsorption capacity of 10.1 cm^3 g^{-1}, higher than IL-NTf_2 (3.6 cm^3 g^{-1}) (Fig. 4a and Supplementary Figs. 30-31), suggesting that PL3(SMF-NTf_2) introduces additional cavities, enhancing permanent porosity.

Photoresponsive PLs offer a promising solution by adjusting gas adsorption properties in response to light, reducing energy consumption during desorption.[59,60] An interesting property of these PLs is their ability to reversibly modulate CO_2 adsorption by light irradiation. Under Vis light irradiation, PL2(SMF-Br) gives the CO_2 uptake of 21.6 cm^3 g^{-1} at 1 bar and 0 °C. Exposing the photoresponsive PLs to UV light reduces CO_2 adsorption. The CO_2 uptake over PL2(SMF-Br) decreases to 15.1 cm^3 g^{-1} after UV irradiation, corresponding to 43.0% of change compared to its uptake under Vis light (Fig. 4b). Meanwhile, the CO_2 uptake over PL3(SMF-NTf_2) shows 21.7% of change under UV irradiation compared to that under Vis irradiation. This significantly lower variation confirms that PL2(SMF-Br) exhibits superior photoresponsivity (Fig. 4b and Supplementary Fig. 31). Cycling performance tests demonstrate that PL2(SMF-Br) maintains stable CO_2 adsorption under both Vis and UV light, highlighting its high cycling stability (Supplementary Fig. 32).

In practical applications, CO_2 is typically found alongside other gases, such as nitrogen (N_2) in flue gas or methane (CH_4) in natural gas reservoirs.[57,61] Effective gas separation requires adsorbents possessing CO_2 selectivity. To assess this, the adsorption of N_2 and CH_4 by PL2(SMF-Br) was evaluated. The results show that under Vis light, PL2(SMF-Br) adsorbs only 0.6 cm^3 g^{-1} of N_2 and 1.2 cm^3 g^{-1} of CH_4 at 1 bar and 0 °C, which is apparently lower than the CO_2 uptake (21.6 cm^3 g^{-1}). When exposed to UV light, only slight change in the uptake of N_2 and CH_4 is observed (Supplementary Figs. 33-36). This indicates that PL2(SMF-Br) exhibits good adsorption selectivity for CO_2 over N_2 and CH_4. By adjusting light conditions, the adsorption capacity for specific gases can be effectively optimized, making PL2(SMF-Br) promising for gas separation and purification applications.

The exceptional CO_2 adsorption performance and tunability promotes us to explore the mechanism. Based on the adsorption capacity of porous host (Supplementary Fig. 37), solvent, and the proportion, the theoretical adsorption capacity of PL2(SMF-Br) is calculated to be 4.2 cm^3 g^{-1}. However, the experimentally measured value reaches 21.6 cm^3 g^{-1}, resulting in an excess adsorption capacity of 17.4 cm^3 g^{-1}. Similarly, for PL3(SMF-NTf_2), the theoretical and measured adsorption capacities are 5.7 cm^3 g^{-1} and 10.1 cm^3 g^{-1}, respectively, with an excess capacity of 4.4 cm^3 g^{-1}. This discrepancy suggests that, in addition to the internal cavities of the porous host, additional external cavities are formed through the packing between the porous host and the sterically hindered solvent in the PLs, leading to the observed excess adsorption capacity. Notably, the SMF exhibits an aggregated distribution in IL-NTf_2 but the in-situ formed MOCs remains nearly monodisperse in IL-Br. This results in a higher number of external cavities in PL2(SMF-Br) than in PL3(SMF-NTf$_2$), explaining the greater increase in actual adsorption capacity relative to the theoretical value for PL2(SMF-Br). MD simulations further validate this hypothesis. The results show that the distance from the trans-MOC center to IL-Br is 9.9 Å, significantly exceeding the trans-MOC radius of 4.3 Å. The difference of 5.6 Å represents the packing distance of the external cavities. Similarly, external cavities size of 6.0 Å is observed in the trans-MOC and IL-NTf$_2$ system. However, since trans-MOC exists in an aggregated state in PL3(SMF-NTf$_2$), its contact area with the sterically hindered solvent is significantly reduced compared to PL2(SMF-Br), leading to a lower number of external cavities in PL3(SMF-NTf$_2$). Upon UV irradiation, azobenzene undergoes trans-to-cis isomerization, leading to a decrease in the MOC–IL-Br distance from 9.9 Å to 6.3 Å. Visual analysis confirms that the trans conformation exhibits a more pronounced external cavity structure (Figs. 4d and 4e). In the PL3(SMF-NTf$_2$) system, external cavity regulation is reflected in the reduction of the MOC–IL-NTf$_2$ distance from 10.3 Å to 9.3 Å. These findings provide direct evidence of the crucial role of azobenzene isomerization in modulating external cavities within PLs system. To quantitatively assess the respective contributions of internal and external cavities in PL2(SMF-Br), CO_2 was used as the probe molecule in the calculations. The pure IL-Br exhibits a free volume of 143.7 Å^3, and that of an isolated MOC cage is 148.2 Å^3. Integration of trans-MOC with IL-Br to form the porous liquid markedly increases the CO_2-accessible free volume to 872.4 Å^3, a value substantially higher than the simple sum of the individual contributions. This additional free volume is primarily attributed to the formation of external cavities (Supplementary Fig. 38).

Durability of PL and generality of in-situ transformation strategy. Durability is an important issue for practical applications. To evaluate the durability of PL2(SMF-Br), characterizations were conducted on the samples stored for one year. The ^{1}H NMR spectrum of the old PL2(SMF-Br) shows no additional peaks compared with the fresh sample, and the characteristic MOC peaks in the ESI-MS spectra remained, indicating that the microstructure of the PL2(SMF-Br) remains stable over time (Supplementary Figs. 39-40). Additionally, CO_2 adsorption experiments were performed to assess the impact of prolonged storage on gas adsorption behavior. The CO_2 adsorption isotherms reveal that the sample maintain a stable CO_2 adsorption capacity over time under Vis light, indicating the retention of their porous structure. Under UV light, a significant decrease in gas adsorption is observed in the old sample, demonstrating that its modulating effect on gas uptake remains intact (Supplementary Fig. 41). These results provide strong evidence of the excellent long-term stability of PL2(SMF-Br), reinforcing its potential for practical applications.

To examine the generality of in-situ transformation strategy for synthesizing different types of PLs through the same porous host, various SMFs (i.e. SMF-2[62] and SMF-3[63]) were employed as porous hosts. ESI-MS and PXRD characterizations confirm their successful synthesis (Supplementary Figs. 42-45), followed by an investigation of their solubility behavior. SMF-2 dissolves in IL-Br, forming PL2(SMF-2-Br). Notably, SMF-2 is insoluble in IL-NTf_2, instead forming a stable suspension, successfully establishing PL3(SMF-2-NTf_2). Similarly, the more compact SMF-3 also dissolves in IL-Br, forming PL2(SMF-3-Br), while remaining insoluble in IL-NTf_2, leading to the formation of a stably dispersed type III PL, PL3(SMF-3-NTf_2) (Supplementary Fig. 46). ^1H NMR characterization was conducted on these four PLs. In PL2(SMF-2-Br) and PL2(SMF-3-Br), the peaks corresponding to the imidazolium component of the ionic liquid shifted upfield to varying degrees (Supplementary Figs. 47-48). In contrast, in PL3(SMF-2-NTf_2) and PL3(SMF-3-NTf_2), the imidazolium peaks shifted downfield (Supplementary Figs. 49-50). This trend is consistent with the behavior observed in SMF-1-based systems, further confirming the generality of the in-situ transformation strategy for controllable synthesizing type II and III PLs using the same porous host.

Discussion

In summary, we report an in-situ transformation strategy to achieve controllable synthesis of type II and type III PLs from the same SMF. The SMF is constructed via the hierarchical self-assembly of MOCs through low-energy ionic bonds, enabling controllable regulation of SMF structural integrity by tuning the electrostatic properties of sterically hindered solvents. This modulation is achieved through ion exchange, replacing Br^- in polyethylene glycol-based ionic liquids with NTf_2^-, generating two distinct sterically hindered solvents, IL-Br and IL-NTf_2. Due to the electrostatic repulsion between SMF and IL-NTf_2, the primary structure of SMF is preserved and the porous host can be dispersed, enabling the successful synthesis of type III PL3(SMF-NTf_2). In contrast, the attractive interactions between IL-Br and SMF disrupt the ionic bonds, facilitates the in-situ transformation of SMF into MOCs, forming type II PL2(SMF-Br) with an high solubility of 150 g L^{-1}—compared with previously reported MOC-based type II PLs (2–62 g L^{-1}). The PL2(SMF-Br) achieves a CO_2 adsorption capacity of 21.6 cm^3 g^{-1} at 0 °C and 1 bar, which is the highest value reported among type II PLs (0.16–13.5 cm^3 g^{-1}). Meanwhile, the CO_2 uptake of its type III counterpart, PL3(SMF-NTf_2), is only 10.1 cm^3 g^{-1}, which is less than half that of PL2(SMF-Br). Moreover, PL2(SMF-Br) inherits the photoresponsive functionality of SMF, exhibiting more than twice higher photoresponsivity than its type III counterpart. The generality of this in-situ transformation strategy is validated through its successful application to different SMFs. These findings might pave the way for the controllable synthesis of PL systems for various applications.

Methods

Synthesis of SMF. The material was synthesized as follows.[64] Cp_2ZrCl_2 (40.0 mg, 0.137 mmol) and H_2BDC-Azo (15.0 mg, 0.055 mmol) were sonicated in a mixture of N,N-dimethylacetamide (DMA, 0.5 mL) and tetrahydrofuran (THF, 0.2 mL). Deionized water (0.4 mL) was then added, and the solution was left undisturbed at room temperature for 3 days, yielding orange cubic crystals. The crystals were washed three times with DMA (3 × 3 mL) to remove any residual ligands and metal salts (23.9 mg, yield 65%). The successful formation of SMF was verified using ESI-MS, PXRD, and SEM analyses, Supplementary Figs. 2–4.

Synthesis of IL-Br and IL-NTf_2. To synthesize IL-Br, polyethylene glycol-400 (PEG-400, 15.0 g, 37.5 mmol) was dissolved in THF (35 mL), followed by the addition of sodium hydroxide

(NaOH, 3.5 g, 87.5 mmol) in water (35 mL). After cooling in an ice-water bath, 4-toluene sulfochloride (TsCl, 16.0 g, 84.0 mmol) was slowly added, and the mixture was stirred at room temperature for 12 h. Subsequently, NaOH (3.0 g, 75.0 mmol) and imidazole (10.0 g, 147.0 mmol) were introduced, and the reaction was refluxed at 80 °C for 12 h until the solution became clear. The product was extracted with dichloromethane, and after solvent removal, a light-yellow PEG-functionalized bis(imidazole) compound was obtained (8.2 g, 15.3 mmol, 40.8% yield based on PEG-400). Next, butyl bromide (11.0 g, 80.3 mmol) and PEG-linked bis(imidazole) (8.2 g, 15.3 mmol) were refluxed in toluene (20 mL) at 80 °C for 24 h under N_2 atmosphere. The resulting product was dissolved in methanol, and residual toluene was removed by evaporation, yielding an orange viscous IL-Br (9.0 g, 11.1 mol, 72.6%). IL-Br (9.0 g, 11.1 mmol) and bistrifluoromethanesulfonimidate ($LiNTf_2$, 16.5 g, 57.5 mmol) were dissolved in a 4:1 (v/v) methanol/water solution and stirred at room temperature for 6 h. The product was extracted three times with dichloromethane (DCM, 3 × 20 mL), and the solvent was removed via vacuum evaporation, yielding IL-NTf_2 (11.4 g, 9.4 mmol, 85%). ^{13}C-NMR spectroscopy was applied to verify the successful formation of IL-Br and IL-NTf_2, Supplementary Figs. 5-6.

Synthesis of PL2(SMF-Br) and PL3(SMF-NTf$_2$). About 70 mg of SMF was dispersed in 5 mL of DCM, followed by adding 1 mL of IL-Br. The mixture was sonicated for 20 min and then dried at 60 °C for 2 h to remove DCM, yielding PL2(SMF-Br). For different concentrations, only the amount of SMF was adjusted, while all other steps remained the same. Unless otherwise specified, the default porous host concentration is 70 g L^{-1}. For the synthesis of PL3(SMF-NTf_2), the procedure followed the same steps as for PL2(SMF-Br), except that IL-Br was replaced with IL-NTf_2. ESI-MS, PXRD, and digital photographs were applied to verify the successful formation of PL2(SMF-Br) and PL3(SMF-NTf_2), Supplementary Figs. 8-9, 11 and Fig 2a.

Gas adsorption measurements. CO_2, CH_4, and N_2 adsorption experiments were conducted using an ASAP 2020 analyzer with 99.999% pure gases. Adsorption isotherms at 0 °C were measured using a thermostatic bath. A xenon lamp (CEL-HXUV300) equipped with 365 nm and 420 nm filters was used as the UV/Vis light source. Prior to measurements, the PLs were evacuated at 80 °C for 6 h, cooled to room temperature, and then irradiated using the xenon lamp for 30 min. The Handheld Solar Power Meter TM-206 was used to measure the intensity of UV and Vis light. The results indicate that the intensity at 365 nm is 0.82 mW cm^{-2}, and at 420 nm it is 4.4 mW cm^{-2}.

Data availability

The data generated in this study are provided in the Supplementary Information/Source Data file. All other relevant data supporting the findings of this study are available from the corresponding author on request.

References

1 Giri, N. et al. Liquids with permanent porosity. *Nature* **527**, 216-220 (2015).

2 Erdosy, D. P. et al. Microporous water with high gas solubilities. *Nature* **608**, 712-718 (2022).

3 Bennett, T. D., Coudert, F.-X., James, S. L. & Cooper, A. I. The changing state of porous materials. *Nat. Mater.* **20**, 1179-1187 (2021).

4 Ma, L. et al. Coordination cages as permanently porous ionic liquids. *Nat. Chem.* **12**, 270-275 (2020).

5 Wang, D. et al. Porous liquids open new horizons: synthesis, applications, and prospects. *Acc. Mate. Res.* **4**, 854-866 (2023).

6 Zhan, G. & Zeng, H. C. Hydrogen spillover through matryoshka-type (ZIFs@)(n-1)ZIFs nanocubes. *Nat. Commun.* **9**, 3778 (2018).

7 Wang, D. C. et al. Shining light on porous liquids: from fundamentals to syntheses, applications and future challenges. *Adv. Funct. Mater.* **32**, 2104162 (2021).

8 Fulvio, P. F. & Dai, S. Porous liquids: The next frontier. *Chem* **6**, 3263-3287 (2020).

9 James, S. L. The dam bursts for porous liquids. *Adv. Mater.* **28**, 5712-5716 (2016).

10 Jie, K., Zhou, Y., Ryan, H. P., Dai, S. & Nitschke, J. R. Engineering permanent porosity into liquids. *Adv. Mater.* **33**, e2005745 (2021).

11 O'Reilly, N., Giri, N. & James, S. L. Porous liquids. *Chem. Eur. J.* **13**, 3020-3025 (2007).

12 Hosono, N., Gochomori, M., Matsuda, R., Sato, H. & Kitagawa, S. Metal-organic polyhedral core as a versatile scaffold for divergent and convergent star polymer synthesis. *J. Am. Chem. Soc.* **138**, 6525-6531 (2016).

13 He, C. et al. A porous metal-organic cage liquid for sustainable CO_2 conversion reactions. *Nat. Commun.* **14**, 3317 (2023).

14 Zhang, J. et al. Porous liquids: a promising class of media for gas separation. *Angew. Chem.*

Int. Ed. **54**, 932-936 (2015).

15 Li, P. et al. Electrostatic-assisted liquefaction of porous carbons. *Angew. Chem. Int. Ed.* **129**, 15154-15158 (2017).

16 Zou, Y. H. et al. Porous metal-organic framework liquids for enhanced CO_2 adsorption and catalytic conversion. *Angew. Chem. Int. Ed.* **60**, 20915-20920 (2021).

17 Zhang, Z. et al. Type II porous ionic liquid based on metal-organic cages that enables *L*-tryptophan identification. *Nat. Commun.* **13**, 2353 (2022).

18 Li, E. et al. Sub-5 Ångstrom porosity tuning in calixarene-derived porous liquids via supramolecular complexation construction. *Angew. Chem. Int. Ed.* **64**, e202421615 (2025).

19 Costa Gomes, M., Pison, L., Cervinka, C. & Padua, A. Porous ionic liquids or liquid metal-organic frameworks? *Angew. Chem. Int. Ed.* **57**, 11909-11912 (2018).

20 Dai, D., Luo, L., Zhu, Q., Wang, D. & Li, T. Preserving macroporosity in type III porous liquids. *Angew. Chem. Int. Ed.* **62**, e202303102 (2023).

21 Lai, B., Crawford, D. E., Wu, H. & James, S. L. Using porous liquids to perform liquid-liquid separations. *Angew. Chem. Int. Ed.* **63**, e202409894 (2024).

22 Li, S., Wang, D., Lee, Y. & Li, T. Preserving mesoporosity in type III porous liquids through dual-layer surface weaving. *Angew. Chem. Int. Ed.* **63**, e202405288 (2024).

23 Chen, H. et al. A bifunctional zeolitic porous liquid with incompatible lewis pairs for antagonistic cascade catalysis. *Chem* **7**, 3340-3358 (2021).

24 He, S. et al. General way to construct micro- and mesoporous metal-organic framework-based porous liquids. *J. Am. Chem. Soc.* **141**, 19708-19714 (2019).

25 Liu, H. et al. A hybrid absorption-adsorption method to efficiently capture carbon. *Nat. Commun.* **5**, 5147 (2014).

26 Knebel, A. et al. Solution processable metal-organic frameworks for mixed matrix membranes using porous liquids. *Nat. Mater.* **19**, 1346-1353 (2020).

27 Bennett, T. D., Coudert, F. X., James, S. L. & Cooper, A. I. The changing state of porous materials. *Nat. Mater.* **20**, 1179-1187 (2021).

28 Mahdavi, H., Smith, S. J. D., Mulet, X. & Hill, M. R. Practical considerations in the design and use of porous liquids. *Mater. Horiz.* **9**, 1577-1601 (2022).

29 Dinker, M. K. et al. Transformation of type III to type II porous liquids by tuning surface rigidity of rhodium(II)-based metal-organic polyhedra for CO_2 cycloaddition. *Angew. Chem. Int. Ed.* **62**, e202306495 (2023).

30 Li, E. et al. Tailoring the gating effect of organic cage via a porous liquid approach. *Adv. Funct. Mater.* **35**, 2413668 (2024).

31 Egleston, B. D. et al. Controlling gas selectivity in molecular porous liquids by tuning the cage window size. *Angew. Chem. Int. Ed.* **59**, 7362-7366 (2020).

32 Chang, C. W. et al. Accelerating solvent selection for type II porous liquids. *J. Am. Chem. Soc.* **144**, 4071-4079 (2022).

33 Jie, K. et al. Transforming porous organic cages into porous ionic liquids via a supramolecular complexation strategy. *Angew. Chem. Int. Ed.* **59**, 2268-2272 (2020).

34 Deng, Z. et al. Facilitate gas transport through metal-organic polyhedra constructed porous

liquid membrane. *Small* **16**, 1907016 (2020).

35 Dinker, M. K. et al. Porous liquids responsive to light. *Angew. Chem. Int. Ed.* **61**, e202212326 (2022).

36 Dinker, M. K. et al. What matters to fabrication of type II porous liquids: A case study on metallocages and bulky ionic liquid? *Small* **20**, 2403174 (2024).

37 Qiu, L. et al. Revolutionizing porous liquids: Stabilization and structural engineering achieved by a surface deposition strategy. *Adv. Mater.* **35**, 2302525 (2023).

38 Tong, Z. et al. Slippery porous-liquid-infused porous surface (SPIPS) with on-demand responsive switching between “defensive” and “offensive” antifouling modes. *Adv. Mater.* **36**, 2308972 (2023).

39 Ning, H. et al. Mechanochemical synthesis of type III porous liquids from solid precursors for the removal and conversion of waste CO_2 from CH_4. *Adv. Mater.* **37**, 2417106 (2025).

40 Li, J. et al. Porous liquids based on ZIF-67@ZIF-8 through the strategy of interface layer reconstruction for CO_2 selective sorption. *Chem. Eng. J.* **500**, 156655 (2024).

41 Li, M. M. et al. Role of cavities created by azobenzene-modified UiO-66 in bulky ionic liquid for high photoresponsive CO_2 uptake behavior. *J. Mater. Chem. A* **11**, 21058-21065 (2023).

42 Mow, R. E. et al. Colloidal three-dimensional covalent organic frameworks and their application as porous liquids. *J. Mater. Chem. A* **8**, 23455-23462 (2020).

43 Tsang, M. Y. et al. Porous liquids as solvents for the economical separation of carbon dioxide from methane. *Mater. Today* **60**, 9-16 (2022).

44 Li, P. et al. Porous liquid zeolites: hydrogen bonding-stabilized H-ZSM-5 in branched ionic liquids. *Nanoscale* **11**, 1515-1519 (2019).

45 Wang, D. et al. Carbon nanotubes and graphene oxide-based solvent-free hybrid nanofluids functionalized mixed-matrix membranes for efficient CO_2/N_2 separation. *Sep. Purif. Technol.* **221**, 421-432 (2019).

46 Li, P. et al. An in situ coupling strategy toward porous carbon liquid with permanent porosity. *Small* **17**, e2006687 (2021).

47 Hayes, R., Warr, G. G. & Atkin, R. Structure and nanostructure in ionic liquids. *Chem. Rev.* **115**, 6357-6426 (2015).

48 MacFarlane, D. R. et al. On the concept of ionicity in ionic liquids. *Phys. Chem. Chem. Phys.* **11**, 4962-4967 (2009).

49 Le Ouay, B. et al. Water-soluble ionic metal-organic polyhedra as a versatile platform for enzyme bio-immobilization. *J. Am. Chem. Soc.* **145**, 11997−12006 (2023).

50 Xin, Y. Y. et al. A novel "pore-carrier transfer" strategy for preparation of porous liquids toward efficient CO_2 capture. *Chem. Eng. J.* **497**, 154765 (2024).

51 Park, J., Sun, L. B., Chen, Y. P., Perry, Z. & Zhou, H. C. Azobenzene-functionalized metal-organic polyhedra for the optically responsive capture and release of guest molecules. *Angew. Chem. Int. Ed.* **53**, 5842-5846 (2014).

52 Ghosh, A., Pruchyathamkorn, J., Fuertes Espinosa, C. & Nitschke, J. R. Light-driven purification of progesterone from steroid mixtures using a photoresponsive metal–organic capsule. *J. Am. Chem. Soc.* **146**, 2568-2573 (2024).

53 Lai, Y. Y. et al. Precise modulation of surface layer dynamics for tunable flowability and gas absorption properties of molecular porous liquids. *Adv. Funct. Mater.* **33**, 2210122 (2023).
54 Li, X. Q. et al. Hierarchical yolk–shell porous Ionic liquids with lower viscosity for efficient C_3H_6/C_3H_8 adsorption and separation. *ACS Appl. Mater. Interfaces* **15**, 51582-51592 (2023).
55 Zhu, Z. et al. High-capacity, cooperative CO_2 capture in a diamine-appended metal–organic framework through a combined chemisorptive and physisorptive mechanism. *J. Am. Chem. Soc.* **146**, 6072-6083 (2024).
56 Kim, E. J. et al. Cooperative carbon capture and steam regeneration with tetraamine-appended metal–organic frameworks. *Science* **369**, 392-396 (2020).
57 Lin, J.-B. et al. A scalable metal-organic framework as a durable physisorbent for carbon dioxide capture. *Science* **374**, 1464-1469 (2021).
58 Sun, Y. et al. Self-assembly of metallacages into multidimensional suprastructures with tunable emissions. *J. Am. Chem. Soc.* **140**, 12819-12828 (2018).
59 Brand, M. C., Rankin, N., Cooper, A. I. & Greenaway, R. L. Photoresponsive type III porous liquids. *Chem. Eur. J.* **29**, e202202848 (2023).
60 Liu, Y. et al. Improving light-responsive efficiency of type II porous liquid by tailoring the functionality of host. *Angew. Chem. Int. Ed.* **64**, e202501191 (2025).
61 Kumar, K. V., Preuss, K., Titirici, M.-M. & Rodríguez-Reinoso, F. Nanoporous materials for the onboard storage of natural gas. *Chem. Rev.* **117**, 1796-1825 (2017).
62 Xiao, Z., Drake, H. F., Rezenom, Y. H., Cai, P. & Zhou, H.-C. Structural manipulation of a zirconocene-based porous coordination cage using external and host–guest stimuli. *Small Struct.* **3**, 2100133 (2022).
63 Liu, G., Ju, Z., Yuan, D. & Hong, M. In situ construction of a coordination zirconocene tetrahedron. *Inorg. Chem.* **52**, 13815-13817 (2013).
64 Yang, T. et al. Photoresponsive supramolecular framework with permanent porosity for controllable CO_2 capture and liberation. *ACS Mater. Lett.* **5**, 3177-3183 (2023).

Acknowledgements

This work was supported by the National Natural Science Foundation of China (22125804 and U24A20534), the Open Research Fund of Suzhou Laboratory (SZLAB-1308-2024-ZD005), and the State Key Laboratory of Materials-Oriented Chemical Engineering (SKL-MCE-24A01) awarded to L.-B.S. We would like to thank Key Laboratory of Nuclear Solid State Physics, Hubei Province, School of Physics and Technology, Wuhan University for providing us the PALS measurements.

Author Contributions

L.-B.S. conceived the research and designed the experiments. Y.L. carried out the sample synthesis and characterization. H.-Y.J., M.-M.L. and T.Y helped with the measurements and analysis. M.Z., C.L. and L.D. performed the MD calculations. L.-B.S. and Y.L. are responsible for the major part of writing this paper, but all authors discussed the results and commented on the various versions of the manuscript.

Competing Interests

The authors declare no competing interests.

Fig. 1 | Schematic diagram for the controllable synthesis of different types of PLs based on the same SMF. a) Self-assembly of metal salts and ligands to MOCs, followed by hierarchical self-assembly of MOCs to SMF, which is used as the porous host. b) Synthesis of type II PL, PL2(SMF-Br), through the dissolution of in-situ transformation SMF to MOCs in sterically hindered solvent IL-Br and synthesis of type III PL, PL3(SMF-NTf$_2$), through the dispersion of SMF in sterically hindered solvent IL-NTf$_2$ as well as their corresponding photographs.

Fig. 2 | Interaction between porous host and solvent. a) PXRD patterns for SMF, PL3(SMF-NTf_2), and PL2(SMF-Br). b) Zeta potential measurements for SMF, IL-NTf_2 and IL-Br. c) Solubility comparison of MOC-based type II PLs. d) Comparison of ^{1}H NMR spectra for IL-Br, PL2(SMF-Br), IL-NTf_2, and PL3(SMF-NTf_2), recorded in DMSO-d_6 at 400 MHz and 25 °C. Interaction energies between e) MOC and Cl^-, f) IL-NTf_2 and MOC, as well as g) IL-Br and MOC. The MOC is represented in a line model.

Fig. 3 | Characterization of type II and type III PLs. The final positional relationship between a) trans-MOC and IL-Br, b) trans-MOC and IL-NTf_2 alongside the analysis of the radial distribution (g(r)), where R represents the radius of cage. c) DTG data of IL-Br, PL2(SMF-Br), IL-NTf_2, and PL3(SMF-NTf_2). d) Temperature-dependent viscosity values for IL-Br, PL2(SMF-Br), IL-NTf_2, and PL3(SMF-NTf_2). e) Oscillation-dependent modulus plots of PL2(SMF-Br) and PL3(SMF-NTf_2) (G′′ for loss modulus, G′ for storage modulus). f) Normalized absorbance changes of PL2(SMF-Br) and PL3(SMF-NTf_2) under UV and Vis light.

Fig. 4 | CO_2 adsorption behavior and mechanism exploration. a) Adsorption isotherms for CO_2 on IL-Br, PL2(SMF-Br), IL-NTf_2, and PL3(SMF-NTf_2). b) Changes in CO_2 adsorption capacity of PL2(SMF-Br), IL-Br, PL3(SMF-NTf_2), and IL-NTf_2 under different light. c) Comparison of CO_2 adsorption capacities of PL2(SMF-Br) with previously reported type II PLs. d) Cavity structure of trans-PL2(SMF-Br) and e) cis-PL2(SMF-Br) analyzed via MD simulation. EC and IC denote external cavities and internal cavities, respectively. The MOC is shown in a line representation, while IL-Br is represented in a stick model.

Editorial Summary

Porous liquids show potential as material for carbon dioxide capture but their controlled synthesis remains challenging. Here the authors report a controlled in-situ transformation strategy to fabricate distinct types of porous liquids from one type of supramolecular framework.

Peer review information: *Nature Communications* thanks Dan Zhao and the other, anonymous, reviewers for their contribution to the peer review of this work. A peer review file is available.

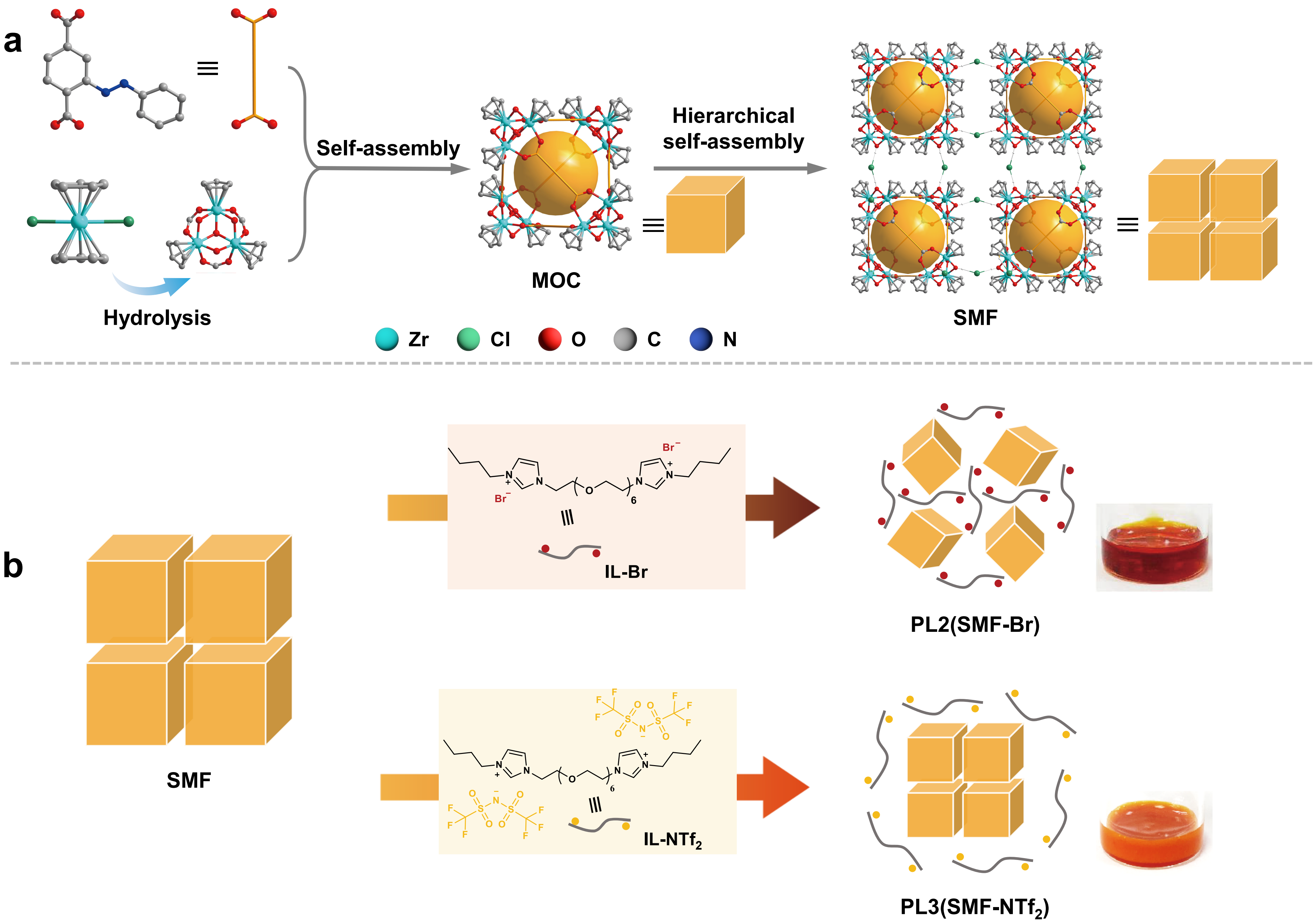
a
≡
Self-assembly
Hierarchical self-assembly
≡
≡
MOC
SMF
Hydrolysis
Zr
Cl
O
C
N
b
SMF
Br⁻
Br⁻
N
N
O
6
|||
IL-Br
PL2(SMF-Br)
F
S
O
N
6
|||
IL-NTf$_2$
PL3(SMF-NTf$_2$)

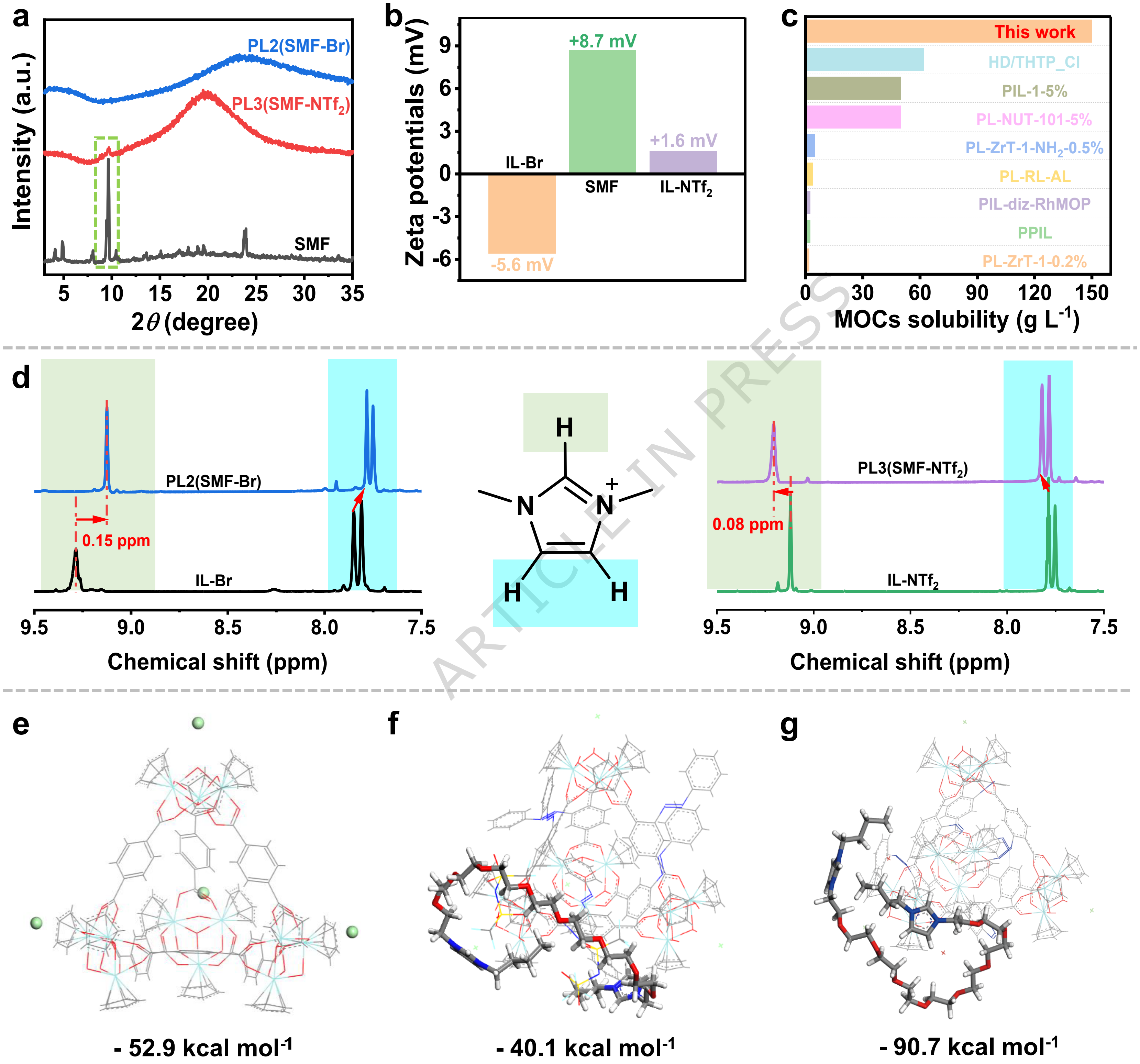
a
Intensity (a.u.)
PL2(SMF-Br)
PL3(SMF-NTf$_2$)
SMF
5
10
15
20
25
30
35
2θ (degree)
b
Zeta potentials (mV)
9
6
3
0
-3
-6
+8.7 mV
+1.6 mV
-5.6 mV
IL-Br
SMF
IL-NTf$_2$
c
This work
HD/THTP_Cl
PIL-1-5%
PL-NUT-101-5%
PL-ZrT-1-NH$_2$-0.5%
PL-RL-AL
PIL-diz-RhMOP
PPIL
PL-ZrT-1-0.2%
0
30
60
90
120
150
MOCs solubility (g L^{-1})
d
PL2(SMF-Br)
0.15 ppm
IL-Br
9.5
9.0
8.5
8.0
7.5
Chemical shift (ppm)
H
N
N
+
H
H
PL3(SMF-NTf$_2$)
0.08 ppm
IL-NTf$_2$
9.5
9.0
8.5
8.0
7.5
Chemical shift (ppm)
e
f
g
- 52.9 kcal mol^{-1}
- 40.1 kcal mol^{-1}
- 90.7 kcal mol^{-1}

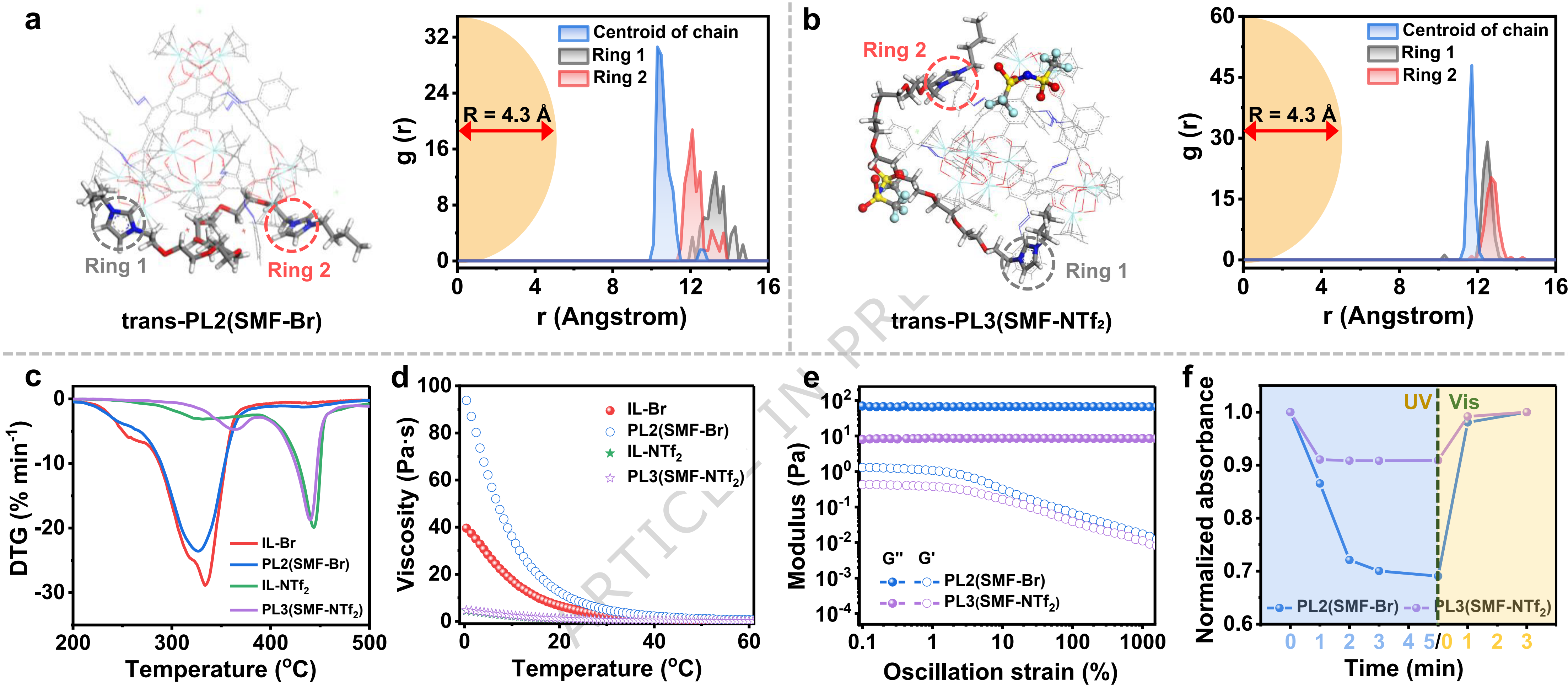
a
Ring 1
Ring 2
trans-PL2(SMF-Br)
Centroid of chain
Ring 1
Ring 2
R = 4.3 Å
g (r)
r (Angstrom)
0
8
16
24
32
0
4
8
12
16
b
Ring 2
Ring 1
trans-PL3(SMF-NTf₂)
Centroid of chain
Ring 1
Ring 2
R = 4.3 Å
g (r)
r (Angstrom)
0
15
30
45
60
c
DTG (% min⁻¹)
Temperature (°C)
IL-Br
PL2(SMF-Br)
IL-NTf₂
PL3(SMF-NTf₂)
0
-10
-20
-30
200
300
400
500
d
Viscosity (Pa·s)
Temperature (°C)
IL-Br
PL2(SMF-Br)
IL-NTf₂
PL3(SMF-NTf₂)
0
20
40
60
80
100
e
Modulus (Pa)
Oscillation strain (%)
G'' G'
PL2(SMF-Br)
PL3(SMF-NTf₂)
10²
10¹
10⁰
10⁻¹
10⁻²
10⁻³
10⁻⁴
0.1
1
10
100
1000
f
Normalized absorbance
Time (min)
UV
Vis
PL2(SMF-Br)
PL3(SMF-NTf₂)
0.6
0.7
0.8
0.9
1.0
0 1 2 3 4 5/0 1 2 3

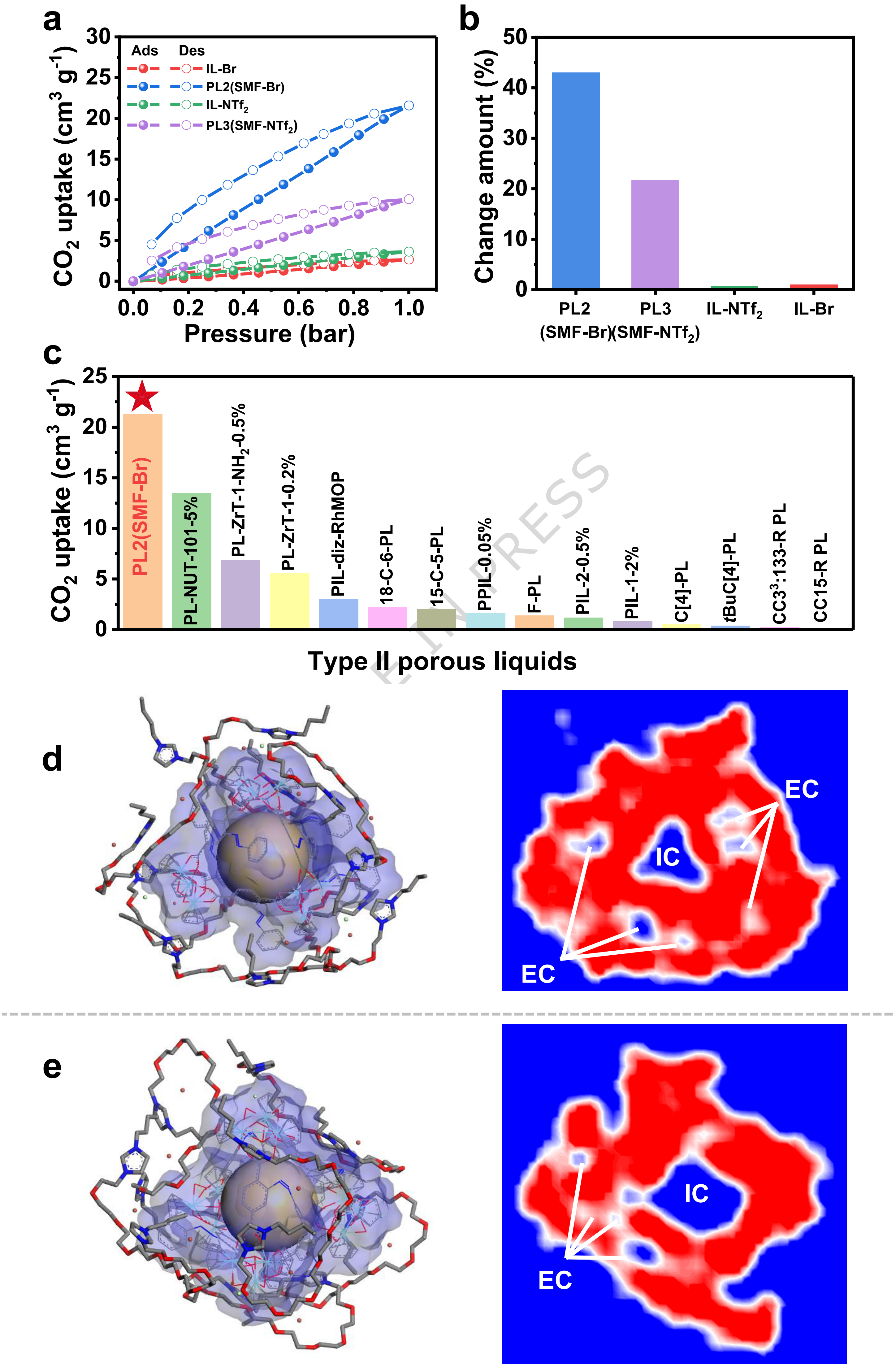
a
Ads
Des
IL-Br
PL2(SMF-Br)
IL-NTf$_2$
PL3(SMF-NTf$_2$)
CO$_2$ uptake (cm^3 g^{-1})
0
5
10
15
20
25
30
0.0
0.2
0.4
0.6
0.8
1.0
Pressure (bar)
b
Change amount (%)
0
10
20
30
40
50
PL2 (SMF-Br)
PL3 (SMF-NTf$_2$)
IL-NTf$_2$
IL-Br
c
CO$_2$ uptake (cm^3 g^{-1})
0
5
10
15
20
25
PL2(SMF-Br)
PL-NUT-101-5%
PL-ZrT-1-NH$_2$-0.5%
PL-ZrT-1-0.2%
PIL-diz-RhMOP
18-C-6-PL
15-C-5-PL
PPIL-0.05%
F-PL
PIL-2-0.5%
PIL-1-2%
C[4]-PL
tBuC[4]-PL
CC3^3:133-R PL
CC15-R PL
Type II porous liquids
d
EC
IC
EC
e
IC
EC